nature materials

ARTICLES

https://doi.org/10.1038/s41563-022-01266-6

Check for updates

Enabling ultra-low-voltage switching in $BaTiO_3$

Y. Jiang[1,2], E. Parsonnet[3], A. Qualls[3], W. Zhao[1], S. Susarla[4], D. Pesquera[1,5], A. Dasgupta[1], M. Acharya[1,2], H. Zhang[1], T. Gosavi[6], C.-C. Lin[6], D. E. Nikonov[6], H. Li[6], I. A. Young[6], R. Ramesh[1,2,3] and L. W. Martin[1,2] ✉

Single crystals of $BaTiO_3$ exhibit small switching fields and energies, but thin-film performance is considerably worse, thus precluding their use in next-generation devices. Here, we demonstrate high-quality $BaTiO_3$ thin films with nearly bulk-like properties. Thickness scaling provides access to the coercive voltages (<100 mV) and fields (<10 kV cm^{-1}) required for future applications and results in a switching energy of <2 J cm^{-3} (corresponding to <2 aJ per bit in a 10 × 10 × 10 nm^3 device). While reduction in film thickness reduces coercive voltage, it does so at the expense of remanent polarization. Depolarization fields impact polar state stability in thicker films but fortunately suppress the coercive field, thus driving a deviation from Janovec–Kay–Dunn scaling and enabling a constant coercive field for films <150 nm in thickness. Switching studies reveal fast speeds (switching times of ~2 ns for 25-nm-thick films with 5-μm-diameter capacitors) and a pathway to subnanosecond switching. Finally, integration of $BaTiO_3$ thin films onto silicon substrates is shown. We also discuss what remains to be demonstrated to enable the use of these materials for next-generation devices.

Ferroelectrics for computing beyond complementary metal oxide semiconductors. The scaling (that is, reduction in size or increase in total number[1]) of bipolar, and then complementary metal oxide semiconductor (CMOS) transistors has been tremendously successful but becomes harder with every generation of the semiconductor process as devices approach fundamental size limits[2]. While Moore's law of scaling has continued, it does so with a much slower reduction in operating voltage since adherence to Dennard's scaling scenario[3] was maintained only until around 2003. Researchers are now exploring alternative approaches to continuing with Moore's law in regard to devices with low operating voltage (<100 mV) and correspondingly low operating energy (1–10 aJ per bit) while maintaining acceptable device switching delay (<0.1 ns). This is driving research on a range of alternative, beyond-CMOS computing pathways (for example, those based on spin, polarization, strain and so on)[4,5]. Ferroelectrics, which could enable both non-volatility and low-read/write energies, are drawing increasing interest for memory (for example, ferroelectric random access memory), logic or logic-in-memory (for example, ferroelectric field-effect transistor (FeFET) applications[6,7], and negative-capacitance field-effect transistors)[8,9]. Despite this interest, the problem is that most ferroelectric devices operate at large voltages[6,7] (>1 V) and are thus incompatible with lower power operation[5]. Solving this problem would mark an important step forward and potentially open a pathway for ferroelectric materials in the advent of beyond-CMOS devices.

From $BaTiO_3$ single crystals to thin films. $BaTiO_3$ is a prototype ferroelectric and, in its single-crystal form, ferroelectric switching can be accomplished with small fields (coercive field ≈ 1 kV cm^{-1}) and energies (~0.1 J cm^{-3}) while maintaining relatively large remanent polarization (≈ 26 μC cm^{-2})[10]. It is also a chemically simple and environmentally benign material that should be under consideration as a candidate for novel low-voltage, non-volatile, ferroelectric-based devices. Such devices, however, require both scaling down of sample thickness (transitioning to ultra-thin films) and (potentially) integration of these materials with existing CMOS technologies. $BaTiO_3$ thin films have been studied widely since the 1970s[11], are readily grown via a variety of methods[10,12–21], and considerable effort has focused on integration of $BaTiO_3$ with silicon platforms[22–26]. The properties of $BaTiO_3$ thin films, however, exhibit large variations and deviations from values measured in single crystals, including larger coercive fields[10,12,14,15,17,19,22,24,25], increased switching energies (that is, the energy required to cycle through the ferroelectric hysteresis loop), and diminished remanent polarization[13,16,18,20,21,26]. Alternative approaches, such as machining of $BaTiO_3$ lamellae from single crystals[27,28], have been explored but, while the resulting lamellae provide properties more comparable to bulk, there are limitations as to how thin they can be made and challenges in regard to their integration into nanoscale devices. Today, there is still a need to realize direct methods to grow such materials with the desired properties (that is, small coercive field, large polarization).

Here, we synthesize epitaxial $BaTiO_3$ films and demonstrate ferroelectric properties that approach those of $BaTiO_3$ single crystals. Structural, chemical, and device fabrication requirements reveal that the best performance is directly correlated to films with an 'idealized' structure. Thickness-scaling studies produce films that exhibit the desired coercive voltages (<100 mV) and fields (<10 kV cm^{-1}). While further reduction in film thickness reduces coercive voltage, it does so at the expense of remanent polarization. Depolarization fields play an important role in regard to properties, but have the fortunate consequence that they suppress the coercive field, leading to deviation from Janovec–Kay–Dunn (JKD) scaling and thickness-independent evolution of coercive field for films <150 nm in thickness. Films also exhibit switching times as short as ~2 ns (25-nm-thick films, 5-μm-diameter capacitors), with lateral-scaling studies revealing a route to subnanosecond switching in devices as large as 10 μm^2. Finally, a pathway to integration on

[1]Department of Materials Science and Engineering, University of California, Berkeley, CA, USA. [2]Materials Sciences Division, Lawrence Berkeley National Laboratory, Berkeley, CA, USA. [3]Department of Physics, University of California, Berkeley, CA, USA. [4]National Center for Electron Microscopy, Molecular Foundry, Lawrence Berkeley National Laboratory, Berkeley, CA, USA. [5]Catalan Institute of Nanoscience and Nanotechnology, CSIC and BIST, Barcelona, Spain. [6]Components Research, Intel Corporation, Hillsboro, OR, USA. ✉e-mail: lwmartin@berkeley.edu

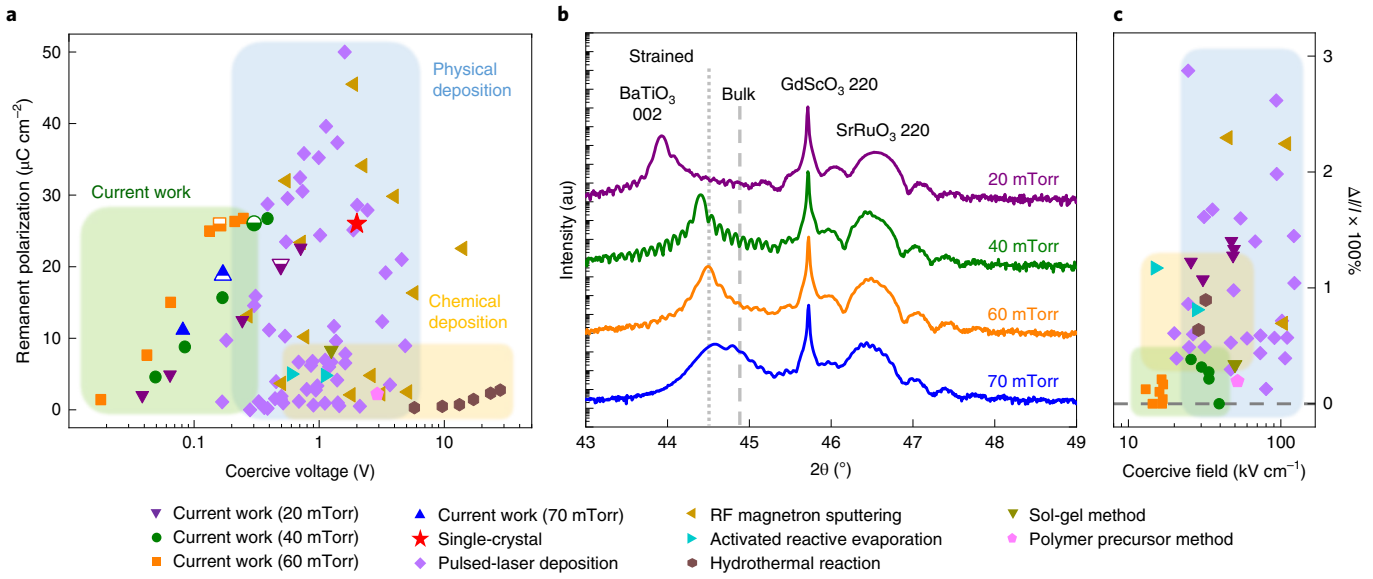

Fig. 1 | Summary of ferroelectric and structural properties of $BaTiO_3$ thin films. a, Comparison of ferroelectricity in $BaTiO_3$ thin films between the current work and that previously reported, via a number of deposition techniques, over the past 50 years. Half-filled symbols represent the ferroelectric properties of 100-nm-thick $BaTiO_3$ thin films at the corresponding growth pressures shown in **b**. **b**, θ–2θ X-ray diffraction scans of 30 nm $SrRuO_3$/100 nm $BaTiO_3$/30 nm $SrRuO_3$/$GdScO_3$ (110) heterostructures with different $BaTiO_3$ growth pressures. Vertical dotted line indicates the theoretical peak position for a $BaTiO_3$ film strained to the $GdScO_3$ substrate, and vertical dashed line indicates the peak position for bulk *c*-oriented $BaTiO_3$. **c**, Comparison of out-of-plane lattice expansion $\Delta l/l$ and coercive field in $BaTiO_3$ thin films between the current work and previously reported ones—those with the least expansion were found to have the lowest coercive fields (and, correspondingly, voltage). au, Arbitrary units.

silicon is shown. We close by discussing what remains to be realized regarding the use of these materials at the length, time, and energy scales required for next-generation devices.

Properties of $BaTiO_3$ films, and metrics requiring consideration. To contextualize this work we review the literature on epitaxial $BaTiO_3$ thin films and demonstrate variability in growth, material quality, structure, and properties reported over the past 50 years (Fig. 1a; see Supplementary Note 1 for references). An important internal calibration is single-crystal $BaTiO_3$ (Fig. 1a), which has small coercive fields (~1 kV cm^{-1}) but relatively large coercive voltage (generally in the range 1–10 V) simply due to the thickness of samples (>10 μm). In part, small coercive fields arise from the fact that electrode–ferroelectric interfaces play a minor role in the overall manifestation of switching behaviour. The same is not true for thin films where interfaces play an increasingly important role as the ferroelectric layer thickness is reduced. An 'ideal' $BaTiO_3$ film would have small coercive voltage and sufficient remanent polarization (that is, <100 mV coercive voltage and 5–10 μC cm^{-2} remanent polarization[5]). Achieving this combination is challenging, and the opposite is often observed in $BaTiO_3$ thin films (Fig. 1a). The films utilized in the current work provide this sought-after combination.

Heterostructures of the form 30 nm $SrRuO_3$/12.5–225 nm $BaTiO_3$/30 nm $SrRuO_3$/$GdScO_3$ (110) and 30 nm $SrRuO_3$/100 nm $BaTiO_3$/30 nm $SrRuO_3$/20 nm $SrTiO_3$/Si (001) were produced via pulsed-laser deposition (Methods), and revealed at least three important materials metrics that are required to produce the desired properties: idealized structure, defect chemistry, and electrode interfaces. Previous studies of ferroelectric films have shown that structural defects (for example, isolated point defects, complexes, or clusters) induced by synthesis can pin domain-wall motion during switching, thus increasing coercivity[14,29,30]. Such defects can also lead to an expansion of the out-of-plane lattice parameter. Defect concentration in pulsed-laser-deposited films is influenced by both the knock-on damage of high-energy adatoms and non-stoichiometric transfer from the target, which are related to laser fluence[14,29] and growth pressure[31]. Increasing growth pressure can enhance the number of scattering events undergone by adatoms as they transit to the substrate, thereby reducing their kinetic energy[24,31] and the potential for knock-on damage. This reduces structural defects (and lattice expansion) and should reduce coercivity (assuming that nucleation is not limited)[14,29–31]. We explored the effect of manipulating the grown-in defect level in $BaTiO_3$ by varying the pressure at which the films are grown, from 20 to 70 mTorr. X-ray diffraction studies revealed changes in structure with this relatively small change in growth pressure (Fig. 1b and Supplementary Fig. 1). For coherently strained films of the same thickness (100 nm), increasing growth pressure from 20 to 60 mTorr led to a decrease in the out-of-plane lattice parameter and, correspondingly, to a decrease in coercive field (for example, the coercive field measured at 1 kHz decreased from 49 to 30 to 16 kV cm^{-1} for growth at 20, 40, and 60 mTorr, respectively; Supplementary Fig. 2). Further increase in growth pressure did not result in further improvement and, for growth at 70 mTorr, the films were partially relaxed (as indicated by two distinct peaks, one related to the strained $BaTiO_3$ and the other to the relaxed, bulk-like $BaTiO_3$; Fig. 1b and Supplementary Fig. 1). This relaxation layer probably produced additional defects within $BaTiO_3$ (ref. [32]) that increased coercive field (17 kV cm^{-1}) and decreased remanent polarization[30] (Fig. 1a and Supplementary Fig. 2). Structural ideality was found to be an important metric for material performance, and can be quantified as the percentage of out-of-plane lattice expansion ($\Delta l/l \times 100\%$) as compared with the theoretical peak position[14,29]. The films here showed the lowest lattice expansion and smallest coercive field (Fig. 1c; see Supplementary Note 1 for references).

In addition to having a nearly ideal structure, the optimized films (grown at 60 mTorr) also exhibited nearly ideal stoichiometry (that is, 1 Ba^{2+}:1 Ti^{4+}; Supplementary Fig. 3) as measured by Rutherford backscattering spectrometry (RBS; Methods). Previous studies have shown that off-stoichiometry induced by purposeful variation of laser fluence during $BaTiO_3$ growth will produce defect–dipole complexes[29] that can not only pin domain-wall motion, causing

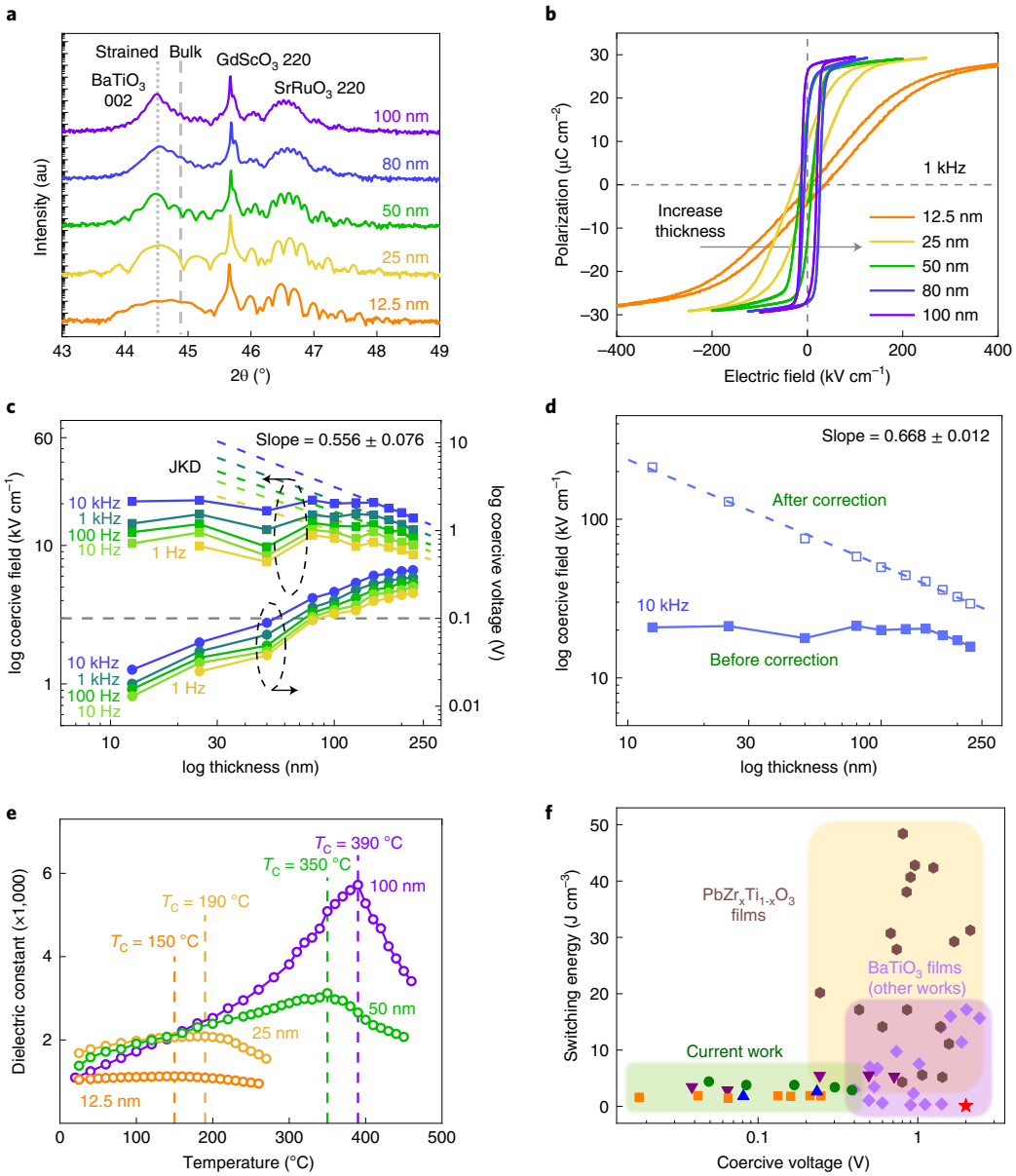

Fig. 2 | Size scaling of $BaTiO_3$ thin films grown at 60 mTorr. a, θ–2θ X-ray diffraction scans of 30 nm $SrRuO_3$/12.5–100 nm $BaTiO_3$/30 nm $SrRuO_3$/$GdScO_3$ (110) heterostructures. The vertical dotted line indicates the theoretical peak position for a $BaTiO_3$ film strained to the $GdScO_3$ substrate, and the vertical dashed line indicates the peak position for bulk *c*-oriented $BaTiO_3$. **b**, Polarization–electric field hysteresis loops measured at 1 kHz as a function of $BaTiO_3$ thickness. **c**, Coercive field (squares, left *y* axis) and voltage (circles, right *y* axis) as a function of $BaTiO_3$ thickness, at frequencies ranging from 1 Hz to 10 kHz. Dashed lines are linear fits for thick films (>150 nm) at different frequencies. The grey dashed line marks the coercive voltage value of 100 mV. **d**, Coercive field (at 10 kHz) as a function of $BaTiO_3$ thickness before (solid squares) and after (hollow squares) depolarization field correction. The dashed line is fit to the traditional JKD scaling law. **e**, Dielectric constant as a function of temperature for $BaTiO_3$ films of thickness 12.5–100 nm. Vertical dashed lines denote the Curie temperature for each film thickness. **f**, Comparison of switching energies between $BaTiO_3$ thin films in the current work and other common ferroelectric materials in the literature. Dark purple triangles, green circles, orange squares, and blue triangles represent $BaTiO_3$ films in the current work grown at 20, 40, 60, and 70 mTorr, respectively; the red star represents $BaTiO_3$ single crystals, light purple diamonds and brown hexagons represent $BaTiO_3$ films and $PbZr_xTi_{1-x}O_3$ films from other previous studies, respectively.

larger coercivity, but also align in the out-of-plane direction, giving rise to an imprint[14,29,30]. Furthermore, it is noted that optimization for layer-by-layer growth using reflection high-energy electron diffraction (RHEED) is not required to achieve the desired properties. As seen for related materials[33], optimization to achieve optimal RHEED oscillations in $BaTiO_3$ did not match the idealized growth conditions required to obtain the desired structure and stoichiometry—instead requiring higher growth temperatures and laser fluence and lower growth pressures. Such conditions resulted in films with expanded out-of-plane lattice parameters, increased coercive fields, and imprinted hysteresis loops. Films grown using these optimized conditions exhibited rather unimpressive RHEED oscillations. This is promising, since such exacting control will not be required and thus further supports the potential translation of this work.

Different electrode fabrication processes and configurations can also affect properties. We focus on 'symmetric' $SrRuO_3$/$BaTiO_3$/$SrRuO_3$ heterostructures, which are known to give some of the best

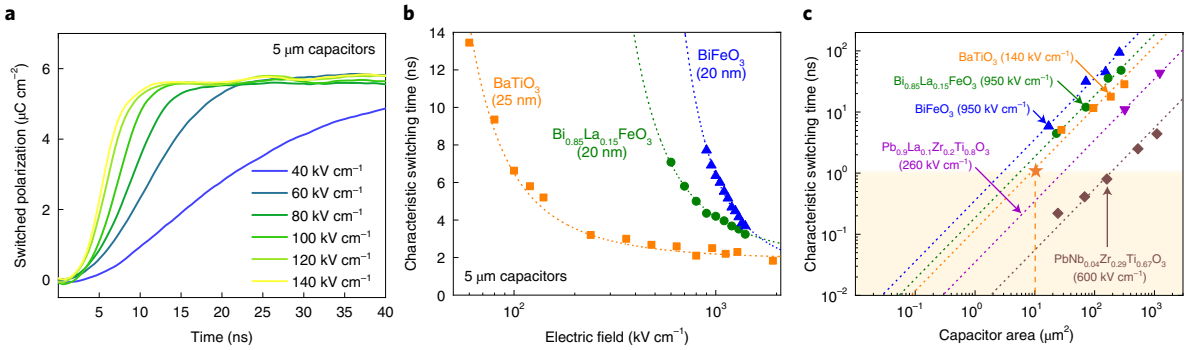

Fig. 3 | Switching-dynamics studies on $BaTiO_3$ thin films grown at 60 mTorr. a, Polarization-transient curves as a function of applied field, measured on 5-μm-diameter circular capacitors. **b**, Extracted characteristic switching time as a function of applied electric field on 5-μm-diameter circular capacitors for 25-nm-thick $BaTiO_3$, 20-nm-thick $BiFeO_3$, and 20-nm-thick $Bi_{0.85}La_{0.15}FeO_3$ films. Dashed curves are fits to Merz's law. **c**, Comparison of characteristic switching time between 25-nm-thick $BaTiO_3$ films in the current work and other common ferroelectric thin films. Dashed lines are linear fits to the data. Orange star denotes the projected capacitor area at which subnanosecond switching time can be achieved. **b**,**c**, Data for other materials are adapted from ref. [54].

properties. Even in such heterostructures, care must be taken in approaching optimal performance. While in most work the $SrRuO_3$ bottom electrode is grown in situ and before the $BaTiO_3$ layer, there is much greater variability in synthesis of the top electrodes (that is, often not $SrRuO_3$, $SrRuO_3$ grown ex situ and then patterned[34], or $SrRuO_3$ grown in situ and then patterned[35]). Here, both ex situ and in situ growth of the $SrRuO_3$ top electrode were explored. With these different processes, although coercive field and remanent polarization are minimally affected the imprint of the hysteresis loop is much larger for ex situ-grown $SrRuO_3$ (Supplementary Fig. 4). For symmetric, in situ-synthesized $BaTiO_3$ heterostructures, high-angle annular dark field diffraction–scanning transmission electron microscopy (STEM) images show pristine interfaces between $BaTiO_3$ and $SrRuO_3$ layers (Supplementary Fig. 5). Despite having identical top and bottom electrode materials, both ex situ and in situ approaches yielded dramatically different results. The ultimate reason for this is a matter for additional study, but it is likely that exposure of the ferroelectric surface to the environment results in chemical and/or structural changes that even a subsequent high-temperature deposition of the top electrode cannot heal. Thus, care must be taken to produce as pristine an interface as is possible to achieve the desired function.

Depolarization fields in thickness scaling. Having established the optimized material and device geometries, we explored the limits of switching and coercive voltage by studying thickness evolution in films of thickness 12.5–225 nm. X-ray diffraction data for $BaTiO_3$ films of thickness 12.5–100 nm (Fig. 2a) and 125–225 nm (Supplementary Fig. 6) revealed that, for all thicknesses, the 002-diffraction condition for these films is located at the position expected for a fully strained film. Furthermore, Laue fringes were observed and provide evidence of high crystallinity and order. Reciprocal space-mapping studies (Supplementary Fig. 7) confirmed that all films were coherently strained to the substrate. Measurement of polarization–electric field hysteresis loops revealed robust polarization. For brevity, data at a single frequency (1 kHz) and for films of thickness 12.5–100 nm are provided (Fig. 2b), but additional frequency-dependent data for all thicknesses are also included (Supplementary Fig. 8). All thicknesses studied exhibit robust saturation polarization (>25 μC cm^{-2}), but remanent polarization reduced as films became thinner (from >25 to <5 μC cm^{-2} for films of thickness <25 nm).

The thickness evolution of coercive field/voltage (as a function of frequency from 1 to 10,000 Hz; Fig. 2c) reveals a difference between thick and thin films. For thicker films (>150 nm), the thickness dependence of coercive field (slope of 0.556) matches that expected for JKD scaling wherein the coercive field $E_C \propto d^{-2/3}$ (where d is film thickness)[36]. In thinner films (<150 nm), the coercive field is essentially independent of thickness. Although JKD scaling happens in many ferroelectrics[25,36,37], there are cases where deviations can exist. For example, interfacial 'dead layers' can give rise to an extra voltage drop and scaling larger than expected (for example, $E_C \propto d^{-1}$)[38], structural changes arising from epitaxial constraints can reduce the energy barrier for switching, producing sub-JKD scaling[37], and changes in the shape of critical nuclei can result in a lack of thickness dependence in ultra-thin films ($d < 15$ nm; this is not the case, however, in these $BaTiO_3$ films)[38]. More often than not, however, deviations from JKD scaling can be attributed to the presence of depolarization fields resulting from incomplete screening[39–41], which can lead to a reduction in the measured coercive field[42]. One can correct for such effects and estimate the actual electric field within the ferroelectric film[42] (Methods), leading to classic JKD scaling (with a slope of 0.668; Fig. 2d).

Thus, depolarization fields play an important role even in films that are nearly 100 nm in thickness. At first glance this is surprising, because seminal theoretical work on related heterostructures showed that ferroelectric order can be maintained down to a thickness of ~2.4 nm[39], and subsequent experiments showed that (given adequate screening of polarization) ferroelectricity could be maintained in films of just a few unit cells in thickness[43,44]. While these works are remembered for setting the ultimate size limits for ferroelectric polarization, they also provide context for these observations and portend challenges in utilization of ultra-thin films. For example, theoretical work also suggested that even under a compressive strain larger than that studied herein, polarization magnitude begins to decrease in films as thick as 15 nm (~38 unit cells) and that polarization is reduced by ~50% in films ~6 nm (~15 unit cells) in thickness[39]. In other words, even well above the critical thickness, depolarization fields reduce the amplitude of polarization and it gradually approaches zero with decreasing thickness, but not in a step-wise manner. Experimentally, the presence of polarization in ultra-thin films was determined (indirectly) by the presence of periodic up- and down-polarized domains[43]—which form to address the large depolarization fields. Thus, in a real electrode/ferroelectric/electrode device with imperfectly screening electrodes, the existence of a depolarization field is likely to be felt even with relatively thick films[41] (that is, >10 nm) and we expect to see effects on polarization, coercive field, and Curie temperature (T_C).

To investigate this, dielectric permittivity was measured as a function of temperature for $BaTiO_3$ thin films of thickness 12.5–100 nm (Fig. 2e). Although the T_C of 100 nm $BaTiO_3$ films grown

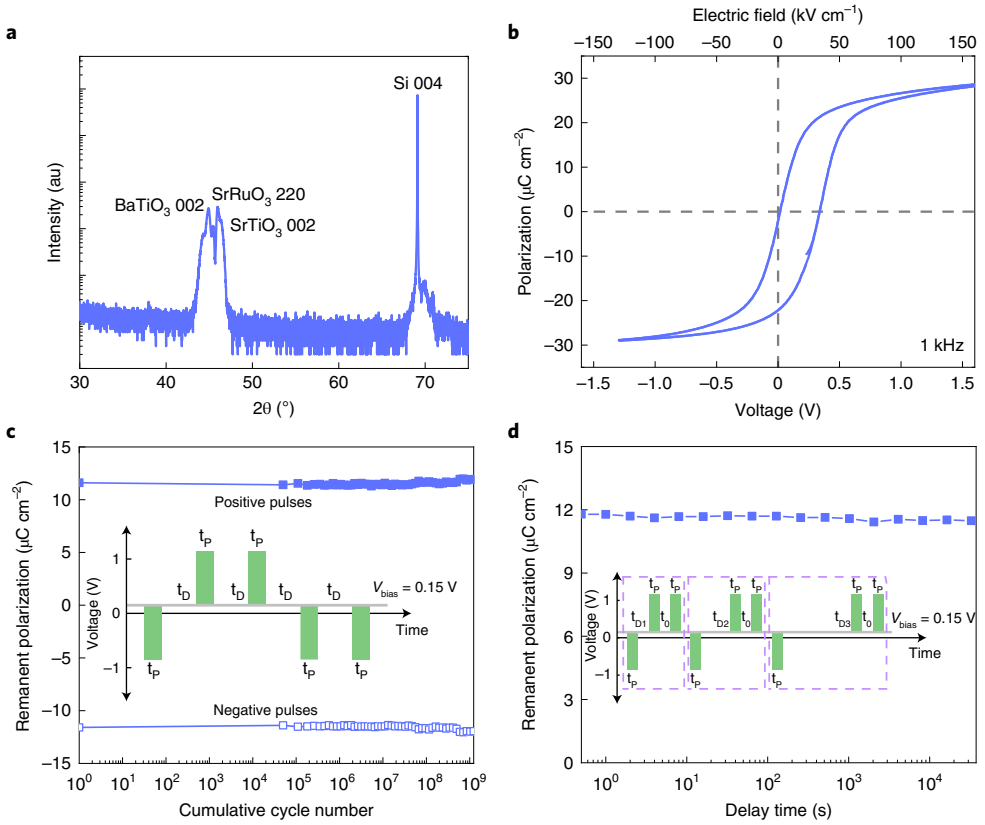

Fig. 4 | Integration of $BaTiO_3$ thin films onto $SrTiO_3$/Si substrates. a, Full-range θ–2θ X-ray diffraction scan of a 30 nm $SrRuO_3$/100 nm $BaTiO_3$/30 nm $SrRuO_3$/20 nm $SrTiO_3$/Si (001) heterostructure. **b**, Polarization–voltage/electric field hysteresis loops of the heterostructure. **c**,**d**, Fatigue (**c**) and retention measurements (**d**) of the heterostructure. Insets, pulse sequences used to probe remanent polarization in fatigue and retention measurements, respectively. The heterostructure is biased at 0.15 V to compensate voltage imprint in the hysteresis loop where t_P is the width of the pulses and is set to be 0.15 ms and t_D, t_{Dn}, and t_0 are the delay times between pulses in corresponding measurements wherein t_D and t_0 are set to be 1 ms while t_{Dn} varies.

on $GdScO_3$ substrates (which approaches 400 °C) is similar to that in previously reported values[14,29,45], as thickness decreases there is a systematic decrease in T_C. In 12.5-nm-thick $BaTiO_3$ films, T_C is reduced to 150 °C (close to that expected for bulk and almost eliminating T_C enhancement induced by −1.0% compressive strain from the substrate[14]), revealing the dramatic effect of depolarization fields on polarization stability and consistent with previous studies[39]. This field also induces polarization reversal after poling, leading to a reduction in remanent polarization (Fig. 2b) consistent with previous studies[41,43]. Piezoresponse force microscopy scans conducted on $BaTiO_3$ thin films confirm the existence of a strong depolarization field (Supplementary Fig. 9) that is directly related to how well the electrodes can screen polarization. While metal oxide electrodes have been shown to be advantageous in alleviating issues of imprint and fatigue[46], 'workhorse' materials like $SrRuO_3$ are, compared with platinum and gold, relatively poor metals. The depolarization field is a function of the quality of the electrode materials (how good a metal they are) and includes aspects of Thomas–Fermi screening length, carrier density/type and so on. Just as there was a concerted effort in the 1990s to identify candidate metal oxide electrodes to enable ferroelectric memories, we may need to revisit a range of materials in this realm of ultra-thin films to identify the materials that best address concerns arising in modern nanoscale devices. Pathways to address these concerns may already be known, including exploration of complex-oxide electrodes with higher carrier densities (thus allowing for better screening) such as certain vanadates, niobates, and molybdates ($SrVO_3$, $SrNbO_3$, and $SrMoO_3$)[47]. Furthermore, computational approaches suggest that smartly designed interfaces can improve ferroelectric stability, including careful control of interface atomic structure and bonding[48,49] and even insertion of interfacial-buffer layers[50]. Ultimately, the time has come to explore these approaches experimentally in ultra-thin films.

While depolarization field can have deleterious effects on remanent polarization and T_C, there are also unintended benefits, such as thickness-independent scaling of coercive fields for films <150 nm in thickness, leading to sub-100 mV operation in films <50 nm in thickness. The result is that these $BaTiO_3$ films, when compared with previous studies of $BaTiO_3$ and $PbZr_xTi_{1-x}O_3$ films, possess lower switching energies (<2 J cm^{-3}, corresponding to <2 aJ per bit in a 10 × 10 × 10 nm^3 device) at all thicknesses while maintaining lower coercive voltages (Fig. 2f; see Supplementary Note 1 for references). For completeness we also investigated fatigue and retention behaviour, both of which indicate robust performance and stability under repeated cycling and time (Supplementary Fig. 10). Taken together, films of thickness 25–50 nm, with their combination of robust remanent polarization (>10 μC cm^{-2}; Fig. 2b and Supplementary Fig. 8) and low coercive voltage (<100 mV; Fig. 2c), are strong candidates to enable low-voltage FeFETs wherein robust polarization is coupled with the channel material to manipulate the threshold voltage of the device[6,51].

Exploring the limit of switching speed in $BaTiO_3$. Besides switching voltage and switching energy, switching speed is also key for ferroelectrics as next-generation non-volatile logic and memories. Since subnanosecond switching has become a target for device applications[5], we explored the limit of switching speed in our $BaTiO_3$ thin films. Switching-dynamics studies were conducted on 25-nm-thick $BaTiO_3$ films using pulse measurements (Methods).

For brevity, here we show the data for polarization-transient curves on 5-μm-diameter capacitors at low applied fields (Fig. 3a), but also provide polarization-transient data on various capacitor sizes at all voltages studied (Supplementary Fig. 11). Characteristic switching times were extracted from polarization-transient curves[52] and plotted as a function of applied field (Fig. 3b). The dashed lines are fits using Merz's law of ferroelectric switching[53], $t_{sw} \propto \exp\left(\frac{\alpha}{E}\right)$, where t_{sw} is the characteristic switching time, α is the activation field, and E is the applied electric field. The 25-nm-thick $BaTiO_3$ films asymptoted to a switching time of ~2 ns with increasing electric field, a value lower than at larger electric fields observed for similar thicknesses of $BiFeO_3$ (~2.4 ns) and $Bi_{0.85}La_{0.15}FeO_3$ (~2.7 ns) films with the same size of capacitors[54]. As the applied field decreased, $BaTiO_3$ heterostructures showed faster switching than other ferroelectrics. Moreover, previous studies on lateral size scaling in capacitor heterostructures have provided a pathway towards the intrinsic-switching regime in ferroelectrics[52,54]. By varying the capacitor diameter (from 5.0 to 18.5 μm) for 25-nm-thick $BaTiO_3$ films, the devices produced switching times similar to other common ferroelectrics[54] but at a much lower electric field/voltage ($E = 140\,kV\,cm^{-1}$, $V = 0.35\,V$; Fig. 3c). The fits (dashed lines) show the evolution of switching time with capacitor area and suggest that 25-nm-thick $BaTiO_3$ films will switch in <1 ns for capacitors with an area of ~10 μm^2 (corresponding to a diameter of ~3.5 μm: orange star, Fig. 3c). Similar lateral size-scaling data for 50- and 100-nm-thick $BaTiO_3$ heterostructures were also acquired (Supplementary Fig. 12) and show nearly identical scaling trends. Thus, it is possible to produce high-quality $BaTiO_3$ films and achieve desired functional performance for new devices (low voltage/power and fast switching).

Integration of $BaTiO_3$ films onto silicon. Finally, to illustrate the potential of this material for applications, we demonstrate a first step towards integrating these materials with silicon. Previous efforts to grow $BaTiO_3$ on silicon or oxide-buffered silicon substrates[17,22–26] resulted in films that appeared to be of good quality by TEM but possessed poor ferroelectric properties (that is, large coercive voltage[17,22,24,25] and small remanent polarization[26]). Here, we explored the possibility of growing $BaTiO_3$ films onto 20-nm-$SrTiO_3$-buffered Si (001) substrates, which are widely available and manufacturable with industry-scale, molecular-beam epitaxy[55]. For brevity, we focus on 100-nm-thick $BaTiO_3$ films (Methods). Because of the large difference in thermal expansion coefficients between perovskite oxides and silicon[25] during cooling after growth, large thermal stresses were formed which manifested in the formation of what appeared to be a mixture of strained, out-of-plane oriented *c* domains and relaxed (bulk-like) out-of-plane polarized *c* domains, as well as in-plane polarized *a* domains (Fig. 4a and Supplementary Fig. 13). These films were more complex than the coherently strained films studied throughout and probably possessed a higher concentration of defects[14,29,30]. Ferroelectric measurements (Fig. 4b), however, revealed similar switching behaviour albeit with a slightly larger coercive field (~16.5 $kV\,cm^{-1}$) than heterostrucures of the same thickness grown on oxide substrates (~16.0 $kV\,cm^{-1}$) and similar to that of $BaTiO_3$ membranes grown on oxide substrates and transferred to silicon (~13 $kV\,cm^{-1}$)[45], while maintaining a relatively large remanent polarization (>10 $\mu C\,cm^{-2}$). A rationalization for these phenomena is provided in Supplementary Note 2. These defects[14,29,30], together with the inhomogeneous strain due to partial relaxation[32], manifested as an unwanted imprint in ferroelectric hysteresis loops. Furthermore, fatigue (Fig. 4c) and retention (Fig. 4d) measurements were nearly identical to those observed for the same thickness of film grown on oxide substrates.

In summary, we have demonstrated the ability to synthesize $BaTiO_3$ thin films with nearly 'intrinsic' ferroelectric properties via pulsed-laser deposition, overcoming a historical trend of diminished properties in such films. Thickness-scaling studies revealed access to low switching voltages (<100 mV) and fields (<10 $kV\,cm^{-1}$), as well as low switching energies (<2 $J\,cm^{-3}$). Switching-dynamics studies revealed fast switching (~2 ns) with a pathway to subnanosecond switching. Similarly good properties were also achieved with integration of $BaTiO_3$ thin films onto silicon. These results show the potential of the use of ferroelectric oxides in low-voltage, low-power, ultra-fast, non-volatile memory and logic devices, perhaps enabling beyond-CMOS devices. $BaTiO_3$ films of thickness 25–50 nm were found to be good candidates for such applications. At the same time, this work suggests that depolarization fields (from incomplete screening with electrodes) still pose a challenge on the thinnest films (due to collapse of remanent polarization) and need to be further addressed to achieve real size scaling in electronic devices. Exploration of oxide electrodes with higher carrier densities, or designing of interfaces between ferroelectrics and electrodes to improve ferroelectric stability, is required to enable the incorporation of ferroelectric materials into next-generation devices.

Online content

Any methods, additional references, Nature Research reporting summaries, source data, extended data, supplementary information, acknowledgements, peer review information; details of author contributions and competing interests; and statements of data and code availability are available at https://doi.org/10.1038/s41563-022-01266-6.

Received: 28 July 2021; Accepted: 20 April 2022;
Published online: 26 May 2022

References

1. Moore, G. E. Cramming more components onto integrated circuits. *Electronics* **38**, 114–117 (1965).
2. Meindl, J. D., Chen, Q. & Davis, J. A. Limits on silicon nanoelectronics for terascale integration. *Science* **293**, 2044–2049 (2001).
3. Dennard, R. H. et al. Design of ion-implanted MOSFET's with very small physical dimensions. *IEEE J. Solid-State Circuits* **9**, 256–268 (1974).
4. Nikonov, D. E. & Young, I. A. Benchmarking of beyond-CMOS exploratory devices for logic integrated circuits. *IEEE J. Explor. Solid-State Comput. Devices Circuits* **1**, 3–11 (2015).
5. Manipatruni, S., Nikonov, D. E. & Young, I. A. Beyond CMOS computing with spin and polarization. *Nat. Phys.* **14**, 338–343 (2018).
6. Mikolajick, T., Schroeder, U. & Slesazeck, S. The past, the present, and the future of ferroelectric memories. *IEEE Trans. Electron Devices* **67**, 1434–1443 (2020).
7. Khan, A. I., Keshavarzi, A. & Datta, S. The future of ferroelectric field-effect transistor technology. *Nat. Electron.* **3**, 588–597 (2020).
8. Salahuddin, S. & Datta, S. Use of negative capacitance to provide voltage amplification for low power nanoscale devices. *Nano Lett.* **8**, 405–410 (2008).
9. Íñiguez, J., Zubko, P., Luk'yanchuk, I. & Cano, A. Ferroelectric negative capacitance. *Nat. Rev. Mater.* **4**, 243–256 (2019).
10. Choi, K. J. et al. Enhancement of ferroelectricity in strained $BaTiO_3$ thin films. *Science* **306**, 1005–1009 (2004).
11. Haertling, G. H. Ferroelectric ceramics: history and technology. *J. Am. Ceram. Soc.* **82**, 797–818 (1999).
12. Yasumoto, T., Yanase, N., Abe, K. & Kawakubo, T. Epitaxial growth of $BaTiO_3$ thin films by high gas pressure sputtering. *Jpn. J. Appl. Phys.* **39**, 5369–5373 (2000).
13. Zhang, W. et al. Space-charge dominated epitaxial $BaTiO_3$ heterostructures. *Acta Mater.* **85**, 207–215 (2015).
14. Damodaran, A. R., Breckenfeld, E., Chen, Z., Lee, S. & Martin, L. W. Enhancement of ferroelectric Curie temperature in $BaTiO_3$ films via strain-induced defect dipole alignment. *Adv. Mater.* **26**, 6341–6347 (2014).
15. Peng, W. et al. Constructing polymorphic nanodomains in $BaTiO_3$ films via epitaxial symmetry engineering. *Adv. Funct. Mater.* **30**, 1910569 (2020).
16. Bhatia, B. et al. High power density pyroelectric energy conversion in nanometer-thick $BaTiO_3$ films. *Nanoscale Microscale Thermophys. Eng.* **20**, 137–146 (2016).
17. Dubourdieu, C. et al. Switching of ferroelectric polarization in epitaxial $BaTiO_3$ films on silicon without a conducting bottom electrode. *Nat. Nanotechnol.* **8**, 748–754 (2013).
18. Iijima, K., Terashima, T., Yamamoto, K., Hirata, K. & Bando, Y. Preparation of ferroelectric $BaTiO_3$ thin films by activated reactive evaporation. *Appl. Phys. Lett.* **56**, 527–529 (1990).

19. Li, A. et al. Fabrication and electrical properties of sol-gel derived $BaTiO_3$ films with metallic $LaNiO_3$ electrode. *Appl. Phys. Lett.* **70**, 1616–1618 (1997).
20. Zhou, Z., Lin, Y., Tang, H. & Sodano, H. A. Hydrothermal growth of highly textured $BaTiO_3$ films composed of nanowires. *Nanotechnology* **24**, 095602 (2013).
21. Lee, E. et al. Preparation and properties of ferroelectric $BaTiO_3$ thin films produced by the polymeric precursor method. *J. Mater. Sci. Lett.* **19**, 1457–1459 (2000).
22. Mazet, L., Yang, S. M., Kalinin, S. V., Schamm-Chardon, S. & Dubourdieu, C. A review of molecular beam epitaxy of ferroelectric $BaTiO_3$ films on Si, Ge and GaAs substrates and their applications. *Sci. Technol. Adv. Mater.* **16**, 036005 (2015).
23. Abel, S. et al. Large Pockels effect in micro-and nanostructured barium titanate integrated on silicon. *Nat. Mater.* **18**, 42–47 (2019).
24. Lyu, J. et al. Control of polar orientation and lattice strain in epitaxial $BaTiO_3$ films on silicon. *ACS Appl. Mater. Interfaces* **10**, 25529–25535 (2018).
25. Scigaj, M. et al. Ultra-flat $BaTiO_3$ epitaxial films on Si (001) with large out-of-plane polarization. *Appl. Phys. Lett.* **102**, 112905 (2013).
26. Drezner, Y. & Berger, S. Nanoferroelectric domains in ultrathin $BaTiO_3$ films. *J. Appl. Phys.* **94**, 6774–6778 (2003).
27. Chang, L., McMillen, M., Morrison, F., Scott, J. & Gregg, J. Size effects on thin film ferroelectrics: experiments on isolated single crystal sheets. *Appl. Phys. Lett.* **93**, 132904 (2008).
28. Chang, L., McMillen, M. & Gregg, J. The influence of point defects and inhomogeneous strain on the functional behavior of thin film ferroelectrics. *Appl. Phys. Lett.* **94**, 212905 (2009).
29. Dasgupta, A. et al. Nonstoichiometry, structure, and properties of $Ba_{1-x}TiO_y$ thin films. *J. Mater. Chem. C Mater.* **6**, 10751–10759 (2018).
30. Saremi, S. et al. Local control of defects and switching properties in ferroelectric thin films. *Phys. Rev. Mater.* **2**, 084414 (2018).
31. Saremi, S. et al. Enhanced electrical resistivity and properties via ion bombardment of ferroelectric thin films. *Adv. Mater.* **28**, 10750–10756 (2016).
32. Catalan, G., Noheda, B., McAneney, J., Sinnamon, L. & Gregg, J. Strain gradients in epitaxial ferroelectrics. *Phys. Rev. B* **72**, 020102 (2005).
33. Breckenfeld, E. et al. Effect of growth induced (non)stoichiometry on interfacial conductance in $LaAlO_3/SrTiO_3$. *Phys. Rev. Lett.* **110**, 196804 (2013).
34. Karthik, J., Damodaran, A. R. & Martin, L. W. Epitaxial ferroelectric heterostructures fabricated by selective area epitaxy of $SrRuO_3$ using an MgO mask. *Adv. Mater.* **24**, 1610–1615 (2012).
35. Weber, D., Vőfély, R., Chen, Y., Mourzina, Y. & Poppe, U. Variable resistor made by repeated steps of epitaxial deposition and lithographic structuring of oxide layers by using wet chemical etchants. *Thin Solid Films* **533**, 43–47 (2013).
36. Kay, H. & Dunn, J. Thickness dependence of the nucleation field of triglycine sulphate. *Philos. Mag.* **7**, 2027–2034 (1962).
37. Xu, R. et al. Reducing coercive-field scaling in ferroelectric thin films via orientation control. *ACS Nano* **12**, 4736–4743 (2018).
38. Jo, J., Kim, Y., Noh, T., Yoon, J.-G. & Song, T. Coercive fields in ultrathin $BaTiO_3$ capacitors. *Appl. Phys. Lett.* **89**, 232909 (2006).
39. Junquera, J. & Ghosez, P. Critical thickness for ferroelectricity in perovskite ultrathin films. *Nature* **422**, 506–509 (2003).
40. Black, C. T. & Welser, J. J. Electric-field penetration into metals: consequences for high-dielectric-constant capacitors. *IEEE Trans. Electron Devices* **46**, 776–780 (1999).
41. Kim, D. et al. Polarization relaxation induced by a depolarization field in ultrathin ferroelectric $BaTiO_3$ capacitors. *Phys. Rev. Lett.* **95**, 237602 (2005).
42. Dawber, M., Chandra, P., Littlewood, P. & Scott, J. Depolarization corrections to the coercive field in thin-film ferroelectrics. *J. Phys. Condens. Matter* **15**, L393–L398 (2003).
43. Fong, D. D. et al. Ferroelectricity in ultrathin perovskite films. *Science* **304**, 1650–1653 (2004).
44. Lee, S. R. et al. First observation of ferroelectricity in ~1 nm ultrathin semiconducting $BaTiO_3$ films. *Nano Lett.* **19**, 2243–2250 (2019).
45. Pesquera, D. et al. Beyond substrates: strain engineering of ferroelectric membranes. *Adv. Mater.* **32**, 2003780 (2020).
46. Morimoto, T. et al. Ferroelectric properties of $Pb(Zi, Ti)O_3$ capacitor with thin $SrRuO_3$ films within both electrodes. *Jpn. J. Appl. Phys.* **39**, 2110–2113 (2000).
47. Oka, D., Hirose, Y., Nakao, S., Fukumura, T. & Hasegawa, T. Intrinsic high electrical conductivity of stoichiometric $SrNbO_3$ epitaxial thin films. *Phys. Rev. B* **92**, 205102 (2015).
48. Duan, C.-G., Sabirianov, R. F., Mei, W.-N., Jaswal, S. S. & Tsymbal, E. Y. Interface effect on ferroelectricity at the nanoscale. *Nano Lett.* **6**, 483–487 (2006).
49. Stengel, M., Vanderbilt, D. & Spaldin, N. A. Enhancement of ferroelectricity at metal–oxide interfaces. *Nat. Mater.* **8**, 392–397 (2009).
50. Lu, H. et al. Enhancement of ferroelectric polarization stability by interface engineering. *Adv. Mater.* **24**, 1209–1216 (2012).
51. Kim, J. Y., Choi, M.-J. & Jang, H. W. Ferroelectric field effect transistors: progress and perspective. *APL Mater.* **9**, 021102 (2021).
52. Li, J. et al. Ultrafast polarization switching in thin-film ferroelectrics. *Appl. Phys. Lett.* **84**, 1174–1176 (2004).
53. Merz, W. J. Domain formation and domain wall motions in ferroelectric $BaTiO_3$ single crystals. *Phys. Rev.* **95**, 690–698 (1954).
54. Parsonnet, E. et al. Toward intrinsic ferroelectric switching in multiferroic $BiFeO_3$. *Phys. Rev. Lett.* **125**, 067601 (2020).
55. Lapano, J. et al. Scaling growth rates for perovskite oxide virtual substrates on silicon. *Nat. Commun.* **10**, 2464 (2019).

Methods

Epitaxial thin film synthesis. $SrRuO_3/BaTiO_3/SrRuO_3/GdScO_3$ (110) heterostructures were synthesized using pulsed-laser deposition (KrF excimer laser, 248 nm; LPX 300, Coherent). Before deposition of $BaTiO_3$ thin films, a 30-nm-thick $SrRuO_3$ thin film was deposited on $GdScO_3$ (110) single-crystal substrate (CrysTech GmBH). The $SrRuO_3$ layer serves as a bottom electrode, and was grown from a $SrRuO_3$ ceramic target at a heater temperature of 690 °C in a dynamic-oxygen pressure of 100 mTorr, at a laser repetition rate of 15 Hz and laser fluence of 1.34 J cm^{-2}. The distance between the target and substrate was maintained at 5.5 cm. Various thicknesses (12.5–225 nm) of $BaTiO_3$ thin films were then deposited from a $BaTiO_3$ ceramic target onto the substrate using the same laser geometry settings, but at a heater temperature of 600 °C in a dynamic-oxygen pressure of 20, 40, 60 or 70 mTorr, at a laser repetition rate of 2 Hz and laser fluence of 1.52 J cm^{-2}. Finally, a 30-nm-thick top $SrRuO_3$ electrode layer was deposited using the same heater temperature, growth pressure, laser fluence and repetition rate as the bottom $SrRuO_3$ layer. Following growth, the whole heterostructure was cooled at a rate of 5 °C min^{-1} under static-oxygen pressure of 760 Torr.

Structural and stoichiometry characterization. θ–2θ X-ray diffraction scans and reciprocal space mapping were carried out with a Panalytical X'pert Pro3 diffractometer (copper $K\alpha_1$, 1.540598 Å) to extract the in-plane and out-of-plane lattice parameters. Stoichiometry of the films was measured using RBS (He-ion beam, National Electrostatics Corp, Model 5SDH pelletron tandem accelerator, incident energy 3.040 MeV, incident angle 22.5°, exit angle 25.35°, scattering angle 168°). For RBS, the $BaTiO_3$ film was grown on an Al_2O_3 substrate to prevent peak overlap between film elements and the rare-earth element from the scandate substrate. Fitting of RBS data was done with SIMNRA software.

Ferroelectric and dielectric measurement. All electrical measurements were performed on circular capacitors, fabricated from the top $SrRuO_3$ electrode via either the in situ method (that is, in situ growth and wet etching using 0.1 M l^{-1} $NaIO_4$ solution) or the ex situ method (that is, MgO hard-mask process). Polarization–electric field/voltage loops were measured using a Precision Multiferroic Tester (Radiant Technologies) at frequencies ranging from 1 Hz to 10 kHz. The coercive field (voltage) E_C (V_C) was extracted by taking the average of the absolute values of positive E_C^+ (V_C^+) and negative E_C^- (V_C^-) (that is, $E_C = (|E_C^+| + |E_C^-|)/2$, $V_C = (|V_C^+| + |V_C^-|)/2$), while remanent polarization was extracted by taking the average of absolute values of positive P_r^+ and negative P_r^- (that is, $P_r = (|P_r^+| + |P_r^-|)/2$) after correction of the loop for any horizontal bias $(E_C^+ + E_C^-)/2$ or $(V_C^+ + V_C^-)/2$. Dielectric constant was measured using an impedance analyser (no. E4990A, Keysight Technologies), by applying a small AC excitation voltage of 5 mV with frequencies ranging from 1 kHz to 100 kHz. $BaTiO_3$ films were pre-poled before dielectric measurement.

STEM. Samples for STEM were mechanically polished at 0.5° and subsequently argon-ion milled using a Gatan Precision Ion milling system, starting from 3.5 keV at 4° down to 1 keV at 1° for the final polish. STEM experiments were carried out using a double-aberration-corrected TEAM I microscope operating at 300 kV, at the National Center for Electron Microscopy, Lawrence Berkeley National Laboratory. The probe semi-angle and beam current used for imaging were 30 mrad and 70 pA, respectively.

Depolarization field correction. As noted in the text, the depolarization field was taken into account to recover the expected JKD scaling law. Using the continuity of electric displacement, we write the actual electric field within the ferroelectric film as[42]

$$E_f = \frac{V + 2P_S\left(\frac{\lambda}{\varepsilon_e}\right)}{d + 2\varepsilon_f\left(\frac{\lambda}{\varepsilon_e}\right)} \quad (1)$$

where V is voltage, P_S is spontaneous polarization, λ is the Fermi screening length of the electrodes, d is film thickness, and ε_f and ε_e are the dielectric constant of the film and electrodes, respectively. In the case of a perfect electrode, $\lambda = 0$, denoting that there is no depolarization field within the system. Thus, the measured coercive field is equal to the actual field in the film (that is, $E_f = V/d$). V and P_S values at 10 kHz can be obtained from the polarization–electric field loops (Fig. 2b and Supplementary Fig. 8). V ranges in value from 0.026 to 0.355 V, while P_S (close to the value of saturation polarization) ranges from 27.8 to 29.9 μC cm^{-2}. The screening length of the $SrRuO_3$ electrode is set as $\lambda = 0.5$ Å, similar in magnitude to other metal electrodes[40]. The dielectric constant of the $SrRuO_3$ electrode, however, is larger than that of simple metals due to contributions from ionic displacement. Here we use $\varepsilon_e = 10\varepsilon_0$ (within the range of previously reported values[40,41]), where ε_0 is the permittivity of the free space. The dielectric constant of the $BaTiO_3$ film was determined from dielectric constant–voltage measurements (Supplementary Fig. 14). ε_f can vary from 135 to 2,300 depending on the applied electric field. In our case, because most electrical measurements were performed with a voltage amplitude of 1 V, which corresponds to a large applied field (for example, >40 kV cm^{-1} in 100 nm film, >75 kV cm^{-1} in 50 nm film, >150 kV cm^{-1} in 25 nm film and >250 kV cm^{-1} in 12.5 nm film), the dielectric constant of the film was estimated to be $\varepsilon_f \approx 360\varepsilon_0$.

Switching-dynamics measurement. Switching-dynamics measurements were performed by applying a sequence of three voltage pulses (Supplementary Fig. 11a) with a pulse generator (Berkeley Nucleonics, no. BN 765) across the $SrRuO_3/BaTiO_3/SrRuO_3$ capacitor structure. The time-dependent displacement current during application of each voltage pulse was measured with an oscilloscope[54]. The first pulse (with an amplitude of −1 V and width of 1 μs) pre-poles the ferroelectric into a negatively polarized state. The second pulse (with variable amplitude and width of 0.5 μs) switches the ferroelectric into a positively polarized state. The third pulse (identical in form to the second) is applied 100 ns after the second to measure the dielectric response of the heterostructure without any switching event. The switching current transient is then obtained by subtracting the dielectric response current of the third pulse from the total current of the second. This gives the displacement current derived from ferroelectric switching alone, which can then be integrated with time to give the polarization transient.

Data availability

All data supporting the findings of this study are available within the article and its Supplementary Information. Additional data are available from the corresponding author upon request.

Acknowledgements

This work was primarily supported by the U.S. Department of Energy, Office of Science, Office of Basic Energy Sciences, Materials Sciences and Engineering Division under contract no. DE-AC02-05-CH11231 (Codesign of Ultra-Low-Voltage Beyond CMOS Microelectronics (MicroelecLBLRamesh)) for the development of materials for low-power microelectronics. E.P., T.G., C.-C.L., D.E.N., H.L., and I.A.Y. acknowledge support from the COFEEE and FEINMAN Programs supported by Intel Corp. W.Z. acknowledges support from the National Science Foundation under grant no. DMR-1708615. D.P. acknowledges support from the European Union's Horizon 2020 research and innovation programme under Marie Skłodowska-Curie grant agreement no. 79712. A.D. acknowledges support from the Army Research Office under ETHOS MURI via cooperative agreement no. W911NF-21-2-0162. M.A. acknowledges support from the Army Research Office under grant no. W911NF-21-1-0118. R.R. and L.W.M. acknowledge additional support of the ARL Collaborative for Hierarchical Agile and Resonant Materials under cooperative agreement no. W911NF-19-2-0119. R.R. also acknowledges support from ASCENT, which is one of the SRC-JUMP Centers. Work at the Molecular Foundry was supported by the Office of Science, Office of Basic Energy Sciences, of the U.S. Department of Energy under Contract No. DE-AC02-05CH11231.

Author contributions

Y.J. and L.W.M. designed the experiments. Y.J. synthesized the thin films. Y.J. and E.P. fabricated the capacitor-based devices. Y.J., E.P., and A.Q. performed the various electrical, dielectric, and ferroelectric measurements. Y.J. completed structural characterization of the materials. S.S. conducted STEM characterization. M.A. conducted RBS measurements. Y.J., E.P., W.Z., D.P., A.D., H.Z., T.G., C.-C.L., D.E.N., and H.L. contributed to the analysis and understanding of data. Y.J. and L.W.M. wrote the core of the manuscript. I.A.Y., R.R., and L.W.M. supervised the research. All authors contributed to the discussion and manuscript preparation and read the final manuscript.

Competing interests

The authors declare no competing interests.

Additional information

Supplementary information The online version contains supplementary material available at https://doi.org/10.1038/s41563-022-01266-6.

Correspondence and requests for materials should be addressed to L. W. Martin.

Peer review information *Nature Materials* thanks Morgan Trassin, Adrian Ionescu and the other, anonymous, reviewer(s) for their contribution to the peer review of this work.

Reprints and permissions information is available at www.nature.com/reprints.